Title

Age- and gender-related differences in cortical geometry and microstructure: Improved sensitivity by regional analysis

Journal

Bone, 52(2)

ISSN

8756-3282

Authors

Kazakia, Galateia J
Nirody, Jasmine A
Bernstein, Gregory
et al.

Publication Date

2013-02-01

DOI

10.1016/j.bone.2012.10.031

Peer reviewed

Published in final edited form as:
Bone. 2013 February ; 52(2): 623–631. doi:10.1016/j.bone.2012.10.031.

Age- and Gender-Related Differences in Cortical Geometry and Microstructure: Improved Sensitivity by Regional Analysis

Galateia J. Kazakia[1], **Jasmine A. Nirody**[1], **Gregory Bernstein**[1,2], **Miki Sode**[1,3], **Andrew J. Burghardt**[1], and **Sharmila Majumdar**[1,3]

[1]Musculoskeletal Quantitative Imaging Research Group, Department of Radiology and Biomedical Imaging, University of California, San Francisco; San Francisco, CA USA

[2]University of California, Berkeley; Berkeley, CA USA

[3]Joint Graduate Group in Bioengineering, University of California, San Francisco and Berkeley; San Francisco and Berkeley, CA USA

Abstract

Objective—While the importance of cortical structure quantification is increasingly underscored by recent literature, conventional analysis techniques obscure potentially important regional variations in cortical structure. The objective of this study was to characterize the spatial variability in cortical geometry and microstructure at the distal radius and tibia using high resolution peripheral quantitative computed tomography (HR-pQCT). We show that spatially-resolved analysis is able to identify cortical sub-regions with increased sensitivity to the effects of gender and aging.

Methods—HR-pQCT scans of 146 volunteers (92 female/54 male) spanning a wide range of ages (20 - 78 years) were analyzed. For each subject, radius and tibia scans were obtained using a clinical HR-pQCT system. Measures describing geometry (cortical bone thickness (Ct.Th)), microstructure (porosity (Ct.Po), pore diameter (Ct.Po.Dm), pore size heterogeneity (Ct.Po.Dm SD)), and cortical bone density were calculated from the image data. Biomechanical parameters describing load and stress distribution were calculated using linear finite element analysis. Cortical quadrants were defined based on anatomic axes to quantify regional parameter variation. Subjects were categorized by gender, and age, and menopausal status for analysis.

Results—Significant regional variation was found in all geometric and microstructural parameters in both the radius and tibia. In general, the radius showed more pronounced and

Corresponding author: Galateia J. Kazakia, Musculoskeletal Quantitative Imaging Research Group, Department of Radiology and Biomedical Imaging, University of California, San Francisco, 185 Berry St, Suite 350, SanFrancisco, CA 94107, Tel: +1 (415) 353-4534, Fax: +1 (415) 353-9423, galateia.kazakia@ucsf.edu.

Author email:
Galateia J. Kazakia galateia.kazakia@ucsf.edu
Jasmine A. Nirody jnirody@gmail.com
Gregory Bernstein gregb@ucsd.edu
Miki Sode msode@mac.com
Andrew Burghardt andrew.burghardt@ucsf.edu
Sharmi la Majumdar sharmila.majumdar@ucsf.edu

Conflict of Interest
None

significant variations in all parameters as compared with the tibia. At both sites, Ct.Po displayed the greatest regional variations. Correlation coefficients for Ct.Po and Ct.Th with respect to load and stress distribution provided evidence of an association between regional cortical structure and biomechanics in the tibia. Comparing women to men, differences in Ct.Po were most pronounced in the anterior quadrant of the radius (36% lower in women ($p<0.01$)) and the posterior quadrant of the tibia (27% lower in women ($p<0.01$)). Comparing elderly to young women, differences in Ct.Po were most pronounced in the lateral quadrant of the radius (328% higher in elderly women ($p<0.001$)) and the anterior quadrant of the tibia (433% higher in elderly women ($p<0.001$)). Comparing elderly to young men, the most pronounced age differences were found in the anterior radius (205% higher in elderly men, ($p<0.001$)) and the anterior tibia (190% higher in elderly men ($p<0.01$)) All subregional Ct.Po differences provided greater sensitivity to gender and age effects than those based on the global means.

Conclusion—These results show significant regional variation in all geometric and microarchitectural parameters studied in both the radius and tibia. Quantification of region-specific parameters provided increased sensitivity in the analysis of age- and gender-related differences, in many cases providing statistically significant differentiation of groups where conventional global analysis failed to detect differences. These results suggest that regional analysis may be important in studies of disease and therapeutic effects, particularly where microstructural parameters based on global analyses have thus far failed to identify a response in bone quality.

Keywords

Cortical bone structure; geometry; porosity; HR-pQCT; regional analysis; age; gender

Introduction

Cortical bone strength is critical to skeletal integrity, particularly at appendicular sites where the cortex is responsible for the majority of axial load transfer [1-2]. Both geometry and microstructure of the cortical compartment are important in determining strength and fracture resistance [3-7]. Highlighting the importance of cortical geometry, cortical thinning has been shown to result in increased fracture incidence in postmenopausal women [8-9]. Cortical porosity, the main microstructural feature of the cortex, is greater at the femoral neck in hip fracture patients than in age-matched controls, and disruption of the normal spatial distribution of cortical porosity is associated with fracture incidence [10-11]. Further, age-related increases in cortical porosity account for more than 75% of the concomitant reduction in cortical strength [12]. Additionally, cortical bone geometry and microstructure are responsive to disease, therapy, and metabolic alterations. For example, increased cortical porosity is associated with chronic kidney disease [13], parathyroid hormone treatment [14], and reduced weight-bearing [15]. Therefore the investigation of cortical geometry and microstructure is an important aspect of understanding biological, pathoetiological, and biomechanical processes occurring within the skeleton.

High resolution peripheral quantitative computed tomography (HR-pQCT) enables 3D visualization of cortical and trabecular structure at the distal radius and tibia at an isotropic nominal resolution of 82 μm. This resolution permits consideration of indices that quantify densitometric, geometric, and microstructural properties of both compartments. Though HR-pQCT cannot resolve cortical porosity at the level of the smallest Haversian and Volkmann canals, the accuracy [16], reproducibility [17], and discriminatory power [16, 18-19] of HR-pQCT cortical indices including thickness and porosity have demonstrated its viability as a tool for evaluation of cortical bone quality. Furthermore, mechanical indices derived from

micro-finite element modeling (μFE) based on HR-pQCT data have also shown high reproducibility in previous studies [20].

While the importance of cortical structure quantification is increasingly underscored by recent literature, conventional analysis techniques obscure potentially important regional parameter variations. To address this, regional analysis can be used to explore anatomic distribution of geometric and microstructural features. Analyses focusing on variation along the length of the bone have found considerable variation in geometry and microarchitecture measures [21-22], as well as correlation between these measures and mechanical competence of bone [22]. In site-specific analyses focused on the trabecular compartment, regional analysis has improved sensitivity to morphologic changes associated with age and gender differences [23] as well as those effected by antiresorptive therapy [24]. Regional analysis has also been used to detect a spatial association between cortical area and stress fracture prevalence at the tibia [25].

In this context, the goal of this study is to characterize the spatial variability in cortical geometry and microstructure at the distal radius and tibia using HR-pQCT. We show that spatially-resolved analysis is able to identify cortical sub-regions with increased sensitivity to the effects of gender and aging.

Methods

Subjects

HR-pQCT image data from the baseline examinations of an ongoing longitudinal patient study were evaluated for this study (Table 1). The subjects consisted of 146 volunteers (92 females age 47.8 ± 15.7 years/54 males age 45.5 ± 16.3 years). Of the 92 women, 46 were post-menopausal. The diversity of the San Francisco Bay Area was reflected in the ethnic composition of the subjects: 47% Caucasian, 44% Asian, 6% Hispanic, and 3% African-American. No bone mineral density (BMD) inclusion/exclusion criteria were used. Subjects with a history of or evidence of metabolic bone disease, as well as those receiving chronic treatment that may affect bone metabolism, were excluded from the study. The study protocol was approved by the UCSF Committee on Human Research, and all subjects gave written informed consent prior to participation.

HR-pQCT imaging

All subjects were imaged in a clinical HR-pQCT system (XtremeCT, Scanco Medical AG, Brüttisellen, Switzerland) using the manufacturer's standard in vivo protocol, described in detail in previous publications [8, 26-27]. The subject's forearm and ankle were immobilized in a carbon fiber cast that was fixed within the gantry of the scanner to minimize motion during imaging. The scan region, spanning 9.02 mm in length and composed of 110 slices, was defined on a single dorsal-palmar projection image of the distal radius/tibia. This region was fixed starting at 9.5 mm for the radius and 22.5 mm for the tibia proximal from the mid-jointline and extending proximally. For tomography, 750 projections were acquired over 180° with a 100-ms integration time at each angular position. The 12.6-cm field of view (FOV) was reconstructed across a 1536 × 1536 matrix using a modified Feldkamp algorithm, yielding 82-μm voxels [28]. Total scan time was 2.8 minutes with an equivalent dose of approximately 3 μSv. Images were inspected for motion-related artifacts, and scans were repeated if necessary. One tibia scan and 6 radius scans were excluded due to excessive motion (quality grading >2 based on the manufacturer's qualitative grading scheme) and/or subject discomfort.

Segmentation algorithm

Image analysis was performed in a customized version of Image Processing Language (IPL v5.08b, Scanco Medical AG) that includes in-house functionality. In this section a segmentation technique used to delineate periosteal and endosteal cortical boundaries is described briefly. Further details on this extended cortical analysis technique can be found in Burghardt et al. [17]. The automated image processing chain is composed of three stages. First, an autocontouring process demarcates the cortical bone compartment. In this stage, a periosteal contour, which separates mineralized bone from extra-osseal soft tissue, and an endosteal contour, which delineates the endocortical boundary from the trabecular compartment, are generated based on an algorithm applying a series of morphological operations. Qualitative inspection of the automatically generated contours is always performed for quality assurance. If a contour visibly deviated from the apparent periosteal or endosteal boundary, minor adjustments are made to the affected region, leaving the remainder of the contour unaffected. In the next step, resolved intra-cortical porosity is distinguished from other features (e.g. erosions or artefactual surface roughness). Finally, the segmented cortical bone and porosity images are combined to generate a refined image of the cortical compartment.

Quantitative Cortical Bone Analysis

Standard measures describing cortical bone density, geometry, and microarchitecture were derived based on the cortical segmentation described above. Apparent cortical bone mineral density (Ct.BMD) is defined as the mean mineralization value for all voxels in the cortical compartment volume of interest (VOI) following a surface erosion of 2 voxels. Cortical tissue mineral density (Ct.TMD) is calculated similarly, but considers only voxels belonging to the mineralized phase. Mean cortical thickness (Ct.Th) is calculated through a 3D sphere filling algorithm [29], neglecting intracortical pore surfaces in local distance calculations. Intracortical pore volume (Ct.Po.V) is the integral volume of all voxels defined as intracortical pore space. Intracortical porosity (Ct.Po) is defined as Ct.Po.V normalized by cortical volume. Finally, the mean cortical pore diameter (Ct.Po.Dm) and standard deviation (Ct.Po.Dm.SD) are calculated from the intracortical pore segmentation by direct 3D methods using maximal spheres [29].

Cortical quadrants were defined based on anatomic axes (Fig. 1), and the associated regional VOI maps were constructed in MATLAB (The MathWorks, Inc., Natick, MA, USA). For the tibia, the reference line connecting the centroids of the tibia and fibula was defined for each slice. The quadrants were placed at a 0° offset to this reference line. For the radius, because the line connecting the centroids of the radius and ulna shifted dramatically within the scanned 9mm span, a different strategy was developed. In this case, the major axis of the radius cross-section was used as the reference line. The radius quadrants were oriented at a 45° offset to the reference line to more appropriately mirror anatomic axes. To obtain parameter values for each quadrant, binary masks of each VOI were overlaid onto maps of cortical metrics calculated from the entire cortical compartment.

μFE Analysis

Linear μFE analysis was applied to calculate apparent biomechanical properties under uniaxial compression. Using a voxel conversion technique [30], the binary image of each radius and tibia was converted to a mesh of isotropic brick elements, each of which was assigned an elastic modulus of 6.8 GPa and a Poisson ratio of 0.3 [31]. To facilitate load distribution calculations, the predefined regions (four cortical quadrants and the trabecular compartment) were labeled as different materials with identical material properties. The models were composed of 1,970,000 elements for the radius and 4,610,000 elements for the tibia, on average. An iterative solver (Scanco FE Software Version 1.12, Scanco Medical)

was used to compute reaction forces at the superior and inferior faces using a uniaxial compression test with an applied strain of 1%. Computations were performed at the UCSF/QB3 Shared Computing Facility, a mixed-architecture Linux HPC grid consisting of 4300 processor cores. No models were excluded due to convergence limitations.

For each model, two metrics were reported for each compartment: 1) mean voxel-level principal stress in the supero-inferior direction and 2) load fraction at the proximal (superior) face. Load fraction was reported as a percent, and denotes the fraction of load in each cortical VOI with relation to the whole segment (four cortical quadrants plus trabecular compartment). For comparison between regional trabecular microstructure and cortical biomechanics, trabecular parameters were calculated using quadrants which consisted of the combination of inner and outer layers for each of four trabecular subregions as created in Sode et al. [23]. These trabecular subregions correspond to the same anatomical axes as our cortical quadrants.

Statistical Analysis

Subjects were categorized by gender, and age, and menopausal status. The elderly cohort included all subjects 65 and older (radius n=9/11 M/F, tibia n=9/13 M/F) while the young cohort included subjects 20 to 29 years of age (radius n=11/14 M/F, tibia n=13/16 M/F). Representative images from each group are provided in Figure 2. Means and standard deviations were calculated for all cortical indices considered and compared by VOI, gender, age, and menopausal status. Using the Shapiro-Wilk W test, it was determined that some indices were not normally distributed. For this reason, non-parametric methods were used for all statistical analyses.

To test the significance of differences between regional parameters and global means, analysis of variance (ANOVA) was performed with subregion as a repeated measure. Subsequently, post-hoc contrast tests were utilized. Specifically, the Wilcoxon rank-sum test for pairwise comparisons with $\alpha = 0.05$ was used to identify the subregions which displayed significant differences. To account for errors due to multiple comparisons, a Bonferroni correction was applied. A Wilcoxon rank-sum test ($\alpha = 0.05$) with Bonferroni correction was also utilized to determine significant differences within each ROI due to gender, age, and menopausal status. The level of statistical significance was set to $p<0.05$. To illustrate the relationship of cortical metrics with age and biomechanical parameters, linear regression analyses were performed, and Spearman's rank correlation coefficients ρ were calculated. All statistical tests were performed using R (v.2.13.0, The R Foundation for Statistical Computing).

Results

Regional Analysis: Spatial Variations in Geometric, Microstructural, and Biomechanical Parameters

Significant regional variation in all geometric and microstructural parameters was found in both the radius and tibia (Table 2, Fig. 3). Males and females displayed the same pattern of regional variation for each parameter. The specific subregions found to have mean values significantly different from the global mean were also generally consistent between genders. Therefore the comparisons described in this section will refer to data inclusive of all subjects. In general, the radius showed more pronounced and significant variations in all parameters as compared with the tibia. At both sites, Ct.Po displayed the greatest regional variations. Ct.BMD displayed the smallest regional variations, on the order of 0 to 3% from the global mean, and therefore is not depicted in Figure 3 nor discussed in relation to age or gender. No significant regional variations in Ct.TMD were observed.

In the radius, the anterior compartment displayed the lowest Ct.Po (−37% from the global mean ($p<0.001$)), while the medial compartment displayed the highest Ct.Po (+37% from the global mean ($p<0.001$)). Mean values of Ct.Po in the medial region were more than double the values in the anterior subregion ($p<0.001$). Ct.Po.Dm and Ct.Po.Dm.SD both followed a pattern similar to that of Ct.Po, with the anterior subregion displaying the smallest and least heterogeneous pore size. Ct.Th was lowest in the lateral (−19% from the global mean ($p<0.001$)), and highest in the anterior and posterior quadrants (+9% ($p<0.05$) and +10% ($p<0.01$) from the global mean, respectively). Ct.BMD was lowest in the lateral quadrant (−3% from the global mean ($p<0.001$)), and highest in the posterior quadrant (+2% from the global mean ($p<0.05$)).

In the tibia, the anterior compartment displayed the lowest Ct.Po (−30% from the global mean ($p<0.001$)), while the posterior-lateral compartments displayed the highest Ct.Po (+17% (NS) and +12% (NS) from the global mean). Mean Ct.Po in the posterior region was 66% higher than Ct.Po in the anterior subregion ($p<0.001$). As in the radius, Ct.Po.Dm and Ct.Po.Dm.SD mirrored the pattern of Ct.Po. Ct.Th was lowest in the anterior region (−14% from the global mean (NS)) and highest in the lateral region (+9% from the global mean ($p<0.001$)) with a significant 13% difference between the two subregions ($p<0.001$). In the tibia, no significant regional variation in Ct.BMD was detected.

Biomechanical parameters exhibited regional variation on a lesser scale than the geometric and microstructural indices. In the radius, mean principal stress ranged from −16% from the global mean (medially, $p<0.001$) to +16% from the global mean (posteriorly, $p<0.001$). Cortical load fraction was highest in the medial quadrant (26% of total bone load) and lowest in the anterior quadrant (15% of total bone load). In the tibia, mean principal stress ranged from −10% from the global mean (posteriorly, $p<0.001$) to +6% from the global mean (anteriorly, $p<0.001$). Cortical load fraction was highest in the lateral quadrant (19% of total bone load) and lowest in the posterior quadrant (15% of total bone load).

Spearman rank correlation coefficients indicated a minimal but significant correlation between Ct.Po and Ct.Th ($\rho = -0.12$, $p<0.001$). Correlation coefficients for Ct.Po and Ct.Th with respect to load and stress distribution provided evidence of an association between both regional cortical and trabecular structure and cortical biomechanics in the tibia (Table 3). Cortical load distribution correlated negatively with trabecular number (Tb.N) ($\rho = -0.28$, $p<0.001$) and positively with heterogeneity of trabecular bone distribution (Tb.Sp.SD) ($\rho = 0.23$, $p<0.001$), while cortical stress distribution displayed the opposite associations ($\rho = 0.22$ with Tb.N, $p<0.001$, and $\rho = -0.21$ with Tb.Sp.SD, $p<0.001$). Though trabecular measures had some effect on biomechanical parameters in the cortex, cortical structure appeared to play the largest role. In particular, Ct.Po was found to contribute primarily to mean stress level ($\rho = 0.56$, $p<0.001$) while Ct.Th was found to contribute primarily to load distribution ($\rho = 0.45$, $p<0.001$). No significant regional associations between structure and biomechanics were found in the radius.

Regional Analysis: Gender Differences

Overall, women had significantly lower Ct.Po based on the global analysis (−21% in the radius ($p<0.01$) and −20% in the tibia ($p<0.05$)) and lower Ct.Th (−10% in the radius ($p<0.001$) and −10% in the tibia ($p<0.001$)) than men. No significant global differences between genders were found in Ct.Po.Dm. and Ct.Po.Dm.SD. Considering the entire population, Ct.Po and Ct.Th were lower in women than in men at all quadrants of the radius and tibia (Fig. 4). Differences in Ct.Po were most pronounced in the anterior quadrant of the radius (−36% in women ($p<0.01$)) and the posterior quadrant of the tibia (−27% in women ($p<0.01$)). In both the radius and the tibia, these subregion gender differences were more pronounced than gender differences based on the global means at the radius (−21% in

women ($p<0.01$)) and tibia (−20% in women ($p<0.05$)). Gender variation in the radius Ct.Po.Dm.SD mirrored that of Ct.Po, with the anterior quadrant showing the greatest difference (−16% in women ($p<0.05$)), while significant gender differences in Ct.Po.Dm were only found in the lateral radius (−4% in women ($p<0.05$)). No significant differences were found in the tibia for either Ct.Po.Dm or Ct.Po.Dm.SD. Gender differences in Ct.Th were most pronounced in the medial and anterior radial quadrants and the medial tibial quadrant. Again, these subregional gender differences were greater than those based on the global means at the radius (−10% in women ($p<0.001$)) and tibia (−10% in women ($p<0.001$)).

Considering only the elderly population (Fig. 4), the same regions show the largest distinctions in Ct.Po between genders, namely the anterior radius (−60% in women ($p<0.001$)) and posterior tibia (−19% in women (NS)). Compared to the entire cohort, the elderly subset showed lower gender differences in Ct.Po, with the notable exception of the anterior radius, where gender differences in Ct.Po *increased* when considering only the elderly group. The anterior radius also showed the greatest gender differences in Ct.Po.Dm (−20% in women ($p<0.01$)) and Ct.Po.Dm.SD (−44% in women ($p<0.001$)). Global analysis of gender differences was unable to detect any significant differences in Ct.Po in this elderly subset. The elderly subset showed greater gender differences in Ct.Th, with the same regions showing maximal differences – the medial and anterior radius and the medial tibia – as in the analysis of the entire cohort. Regional Ct.Th in this elderly subset provided increased sensitivity to gender differences compared to the global analysis at the radius (−16% in women (NS)) and tibia (−17% in women ($p<0.05$)).

Regional Analysis: Age Differences

In a pooled analysis of males and females, elderly subjects had significantly higher Ct.Po based on the global analysis (+131% in the radius ($p<0.001$) and +181% in the tibia ($p<0.001$)) and lower Ct.Th (−13% in the radius ($p<0.05$) and −12% in the tibia ($p<0.01$)) than the young cohort. A lower Ct.Po.Dm.SD was found in elderly subjects only in the radius (−17% ($p<0.05$)), and there were no significant differences between age groups for Ct.Po.Dm. Ct.Po and age were positively correlated at both sites ($\rho=0.53$ ($p<0.001$) in the radius, 0.62 ($p<0.001$) in the tibia), while Ct.Th and age were negatively correlated ($\rho=-0.30$ ($p<0.001$) in the radius, −0.29 ($p<0.05$) in the tibia).

Age-related changes were greater in women than in men for all regions at both sites (Table 2, Fig. 5). Comparing elderly to young women, elderly women displayed significantly elevated Ct.Po and significantly decreased Ct.Th at all quadrants of both radius and tibia. Porosity differences were most pronounced in the lateral quadrant of the radius (+328% in elderly women ($p<0.001$)) and the anterior quadrant of the tibia (+433% in elderly women ($p<0.001$)). These subregion Ct.Po changes were more pronounced than those based on the global means at the radius (+206% in elderly women ($p<0.001$)) and the tibia (+297% in elderly women ($p<0.001$)). Elderly women showed the greatest increase in Ct.Po.Dm and Ct.Po.Dm.SD in the lateral radius (+19% for Ct.Po.Dm ($p<0.01$) and +36% for Ct.Po.Dm.SD ($p<0.01$)). Sensitivity to age in women was highest in the lateral tibia for Ct.Po.Dm (+21% for elderly women ($p<0.01$)), and in the anterior tibia for Ct.Po.Dm.SD (+37% for elderly women ($p<0.01$)). The highest sensitivity to aging in Ct.Th was observed in the lateral quadrant of both the radius (−22% ($p<0.01$) in elderly women vs. −20% globally ($p<0.01$)) and tibia (−19% ($p<0.01$) in elderly women vs. −17% globally ($p<0.01$)). Both Ct.Po and thickness were more highly correlated with age in women than in men (Table 4).

Comparing women by menopausal status, postmenopausal women displayed significantly elevated Ct.Po and significantly decreased Ct.Th at all quadrants of both radius and tibia.

Porosity differences were most pronounced in the anterior quadrant of the radius (+126% in postmenopausal women ($p<0.001$)) and the anterior quadrant of the tibia (+261% in postmenopausal women ($p<0.001$)) These subregional Ct.Po differences were more pronounced than those based on the global means at the radius (+99% in postmenopausal women ($p<0.001$)) and the tibia (+148% in postemenopausal women ($p<0.001$)). Differences in Ct.Po.Dm. and Ct.Po.Dm.SD were, similarly to Ct.Po., highest in the anterior tibia (+11% in Ct.Po.Dm ($p<0.001$) and +18% in Ct.Po.Dm.SD ($p<0.001$)). No significant differences with menopausal status for these parameters were found in the radius. The most pronounced differences in Ct.Th were found in the posterior radius (−18% ($p<0.001$) vs. −17% globally ($p<0.001$)) and the lateral tibia (−13% ($p<0.001$) vs. −11% globally ($p<0.001$)).

Comparing elderly to young men, increased Ct.Po was evident in every quadrant of the radius and tibia (Fig. 5) As was seen when comparing women by menopausal status, the most pronounced age differences were found in the anterior radius (+205% in elderly men, ($p<0.001$)) and the anterior tibia (+190% in elderly men ($p<0.01$)) Again, subregional Ct.Po changes provided greater sensitivity to age effects than those based on the global means at the radius (+78% in elderly men ($p<0.001$)) and tibia (+107% in elderly men ($p<0.001$)). The greatest sensitivity to age effects in men for Ct.Po.Dm and Ct.Po.Dm.SD was seen in the anterior radius (+39% for Ct.Po.Dm ($p<0.001$) and +77% for Ct.Po.Dm.SD ($p<0.001$) and posterior tibia (+29% for Ct.Po.Dm ($p<0.01$) and +30% for Ct.Po.Dm.SD ($p<0.05$)). Increased sensitivity to age was also evident in the regional analysis of Ct.Th, for which the most pronounced age differences were found in the lateral radius (−11% (NS) vs. −4% globally (NS)) and tibia (−16% ($p<0.05$) vs. −6% globally (NS)).

Discussion

This study documented the spatial variability in cortical geometry and microstructure at the distal radius and tibia using HR-pQCT. Our results illustrate that the investigation of regional changes provides increased sensitivity to age- and gender-related skeletal adaptations.

Spatial heterogeneity in porosity was particularly pronounced. Elevated Ct.Po was detected at the medial radius and the posterior-lateral tibia, both of which are adjacent to the secondary bone (ulna and fibula, respectively). This phenomenon could be secondary to the biomechanical influence of load sharing between bones. Decreased cortical bone quality in response to reduced loading is supported by studies describing increased porosity [15, 32-33] and decreased cortical density [34-38] under conditions of reduced loading. Regional μFE analysis did not provide evidence of decreased loading at the medial radius or the posterior-lateral tibia; however, the μFE models do not incorporate secondary structures or soft tissues and therefore cannot capture the influence of load sharing on the distribution of biomechanical parameters. A second consideration is the location of ligament, tendon, and membrane attachments. Within the scanned regions of the radius and tibia, no ligament or tendon insertions exist. The interosseous membrane does have a surface attachment within the scanned region, effecting load transfer between bones. A third consideration in the interpretation of increased porosity is the distribution of the vasculature. Vessel distribution in the distal radius and tibia is nonuniform, with the greatest concentration of intracortical vasculature in quadrants adjacent to the secondary bones [39-42]. A portion of Ct.Po heterogeneity is likely driven by this vascular anatomy.

Previous studies of cortical bone distribution at the tibia have been restricted to the evaluation of densitometric and geometric parameters [25, 43-45]. Results from these studies indicate that cortical BMD is maximal in the posterior region of the tibia, which is

contradictory to our findings of 1) no significant regional variation in Ct.BMD and 2) maximal porosity in the posterior tibia. The regional distribution of Ct.Th reported in these studies also contradicts our findings. Importantly, the scan locations are distinct and likely account for these discrepancies. While our HR-pQCT measurements are made in the ultra-distal tibia, the earlier pQCT studies were performed closer to the mid-shaft of the tibia. Regional distribution of geometric and microstructural properties at the tibia is sensitive to and must be interpreted in the context of the specific analysis site.

Spatial variability in cortical parameters was, in general, lower than that documented within the trabecular compartment of the same cohort [23]. Importantly, however, regional discrimination of gender and age effects (particularly for Ct.Po) were substantially larger than obtained through trabecular analysis. For example, a 55% difference between elderly and young women was detected by trabecular heterogeneity, the trabecular structure index that best differentiated elderly from young women [23]. Our analysis of Ct.Po resulted in a 443% difference between elderly and young women (at the anterior tibia). Similarly, a 48% difference between genders was detected in the elderly cohort by trabecular heterogeneity [23], whereas Ct.Po detected a 60% difference between genders (at the anterior radius). Comparison of correlation coefficients for cortical parameters and age with those for trabecular parameters and age as reported by Sode et al. corroborates this greater effect size in cortical parameters.

Gender analysis showed that Ct.Po and Ct.Th are lower in women in every quadrant of both the radius and the tibia, consistent with prior reports based on global analysis [1, 18, 22]. The finding that women display higher sensitivity to aging in all quadrants is also consistent with studies considering Ct.Th. in the distal radius [22]. Regional analysis showed that the anterior radius was particularly sensitive to gender differences in the elderly cohort, whereas the global analysis could not detect gender differences in this cohort. Increased regional sensitivity to gender differences in the elderly cohort was driven by porosity acceleration at the anterior radius in particular in men in the later decades (Fig. 6).

Increased sensitivity to the effects of aging was evident in the anterior radius and anterior tibia in both men and women. Similarly, in a study of bone response to immobilization, the anterior tibial diaphysis experienced the largest decrease in cortical density [46]. This evidence suggests that focused regional analysis – perhaps of the anterior tibia specifically – may increase sensitivity in the study of biological response and fracture prediction beyond the context of age- and gender-related differences.

Biomechanical parameters were assessed in an effort to clarify local relationships between mechanics and bone structure. In the tibia, Ct.Po was positively correlated with tissue-level stress, suggesting that porosity may act as a local stress riser within cortical tissue. Tissue-level stress/strain distributions from linear finite element models have correlated well with observed microdamage [47], indicating that the microenvironment associated with high Ct.Po may initiate fracture. Load distribution within the cortex, on the other hand, was primarily driven by Ct.Th. A positive association indicated preferential load distribution through regions of the cortex with greatest thickness. Given that there exists significant spatial variation in trabecular structure, regional trabecular microstructure can be expected to also play a role in cortical biomechanics. Indeed, trabecular measures also correlated with cortical biomechanical parameters in the tibia, though not quite as strongly as cortical measures. Trabecular number (Tb.N), in particular, was found to have a relatively strong negative correlation with load distribution and a positive correlation with stress distribution, while heterogeneity of trabecular bone distribution (Tb.Sp.SD) showed the opposite pattern. A full discussion of regional variations in trabecular geometry and microstructure can be found in Sode et al. [23]. In the radius, no regional association was found between

biomechanical parameters and bone structure. The distal radius site has a flared metaphyseal geometry, with a periosteal perimeter that increases dramatically towards the joint line. It may be that this feature – more than Ct.Po or Ct.Th - determines load and stress distribution in the radius.

There are limitations in the study design worth considering. First, the lack of longitudinal data limits the power of observations related to age effects. However, the cross-sectional design enabled a large range of ages to be studied and made possible comparisons based on menopausal status. Second, the region definition described in this study was arbitrary. However, the orientation of quadrants was systematic, consistent with anatomic axes, and unaffected by subject positioning. The fact that different anatomic regions showed variable bone quality response to biological effects suggests that a context- and knowledge-driven approach to focal analysis should be explored. Third, the endocortical boundary definition used in this analysis may exclude potential zones of trabeculated cortex, particularly in elderly subjects. However, exclusion of these zones would provide conservative estimates of age- and gender-related differences. Were the endocortical boundary to include all trabeculated cortex, differences between low and high porosity cohorts could be even larger than reported here.

In conclusion, we found significant regional variation in all geometric and microarchitectural parameters studied in both the radius and tibia. Quantification of region-specific parameters provided increased sensitivity in the analysis of age- and gender-related differences, in many cases providing statistically significant differentiation of groups where conventional global analysis failed to detect differences. These results suggest that regional analysis may be important in studies of disease and therapeutic effects, particularly where microstructural parameters based on global analyses have thus far failed to identify a response in bone quality.

Acknowledgments

The authors thank Willy Tjong and Janina Patsch, MD, PhD for critical discussion and technical assistance. This publication was supported by NIH K01 AR056734 (GJK), NIH R01 AG017762 (SM), NIH R01 AR060700 (AJB), and the UC Berkeley Undergraduate Research Apprentice Program (GJK, GB).

References

1. Burghardt AJ, Kazakia GJ, Ramachandran S, Link TM, Majumdar S. Age- and gender-related differences in the geometric properties and biomechanical significance of intracortical porosity in the distal radius and tibia. J Bone Miner Res. 2010; 25:983–993. [PubMed: 19888900]
2. MacNeil JA, Boyd SK. Load distribution and the predictive power of morphological indices in the distal radius and tibia by high resolution peripheral quantitative computed tomography. Bone. 2007; 41:129–137. [PubMed: 17442649]
3. Augat P, Schorlemmer S. The role of cortical bone and its microstructure in bone strength. Age Ageing. 2006; 35:27–31.
4. Augat P, Reeb H, Claes LE. Prediction of fracture load at different skeletal sites by geometric properties of the cortical shell. Journal of Bone and Mineral Research. 1996; 11:1356–1363. [PubMed: 8864911]
5. Schaffler MB, Burr DB. Stiffness of compact bone: effects of porosity and density. Journal of Biomechanics. 1988; 21:13–16. [PubMed: 3339022]
6. Currey JD. The effect of porosity and mineral content on the Young's modulus of elasticity of compact bone. Journal of Biomechanics. 1988; 21:131–139. [PubMed: 3350827]
7. Voide R, Schneider P, Stauber M, van Lenthe GH, Stampanoni M, Muller R. The importance of murine cortical bone microstructure for microcrack initiation and propagation. Bone. 2011; 49:1186–1193. [PubMed: 21884836]

8. Sornay-Rendu E, Boutroy S, Munoz F, Delmas PD. Alterations of cortical and trabecular architecture are associated with fractures in postmenopausal women, partially independent of decreased BMD measured by DXA: the OFELY study. J Bone Miner Res. 2007; 22:425–433. [PubMed: 17181395]

9. Melton LJ 3rd, Christen D, Riggs BL, Achenbach SJ, Muller R, van Lenthe GH, Amin S, Atkinson EJ, Khosla S. Assessing forearm fracture risk in postmenopausal women. Osteoporos Int. 2010; 21:1161–1169. [PubMed: 19714390]

10. Barth RW, Williams JL, Kaplan FS. Osteon Morphometry in Females with Femoral-Neck Fractures. Clin Orthop Relat R. 1992:178–186.

11. Bell KL, Loveridge N, Power J, Garrahan N, Meggitt BF, Reeve J. Regional differences in cortical porosity in the fractured femoral neck. Bone. 1999; 24:57–64. [PubMed: 9916785]

12. McCalden RW, McGeough JA, Barker MB, Court-Brown CM. Age-related changes in the tensile properties of cortical bone. The relative importance of changes in porosity, mineralization, and microstructure. Journal of Bone and Joint Surgery. American Volume. 1993; 75:1193–1205.

13. Leonard MB. A Structural Approach to Skeletal Fragility in Chronic Kidney Disease. Semin Nephrol. 2009; 29:133–143. [PubMed: 19371804]

14. Burr DB, Hirano T, Turner CH, Hotchkiss C, Brommage R, Hock JM. Intermittently administered human parathyroid hormone(1-34) treatment increases intracortical bone turnover and porosity without reducing bone strength in the humerus of ovariectomized cynomolgus monkeys. Journal of Bone and Mineral Research. 2001; 16:157–165. [PubMed: 11149480]

15. Tjong, W.; Sode, M.; Carballido-Gamio, J.; Burghardt, A.; Majumdar, S.; Feeley, B.; Ma, CB.; Kazakia, G. Longitudinal HR-pQCT assessment of the influence of reduced weight bearing on bone structure and mechanics. European Calcified Tissue Society; Athens, Greece: 2011.

16. Nishiyama KK, Macdonald HM, Buie HR, Hanley DA, Boyd SK. Postmenopausal women with osteopenia have higher cortical porosity and thinner cortices at the distal radius and tibia than women with normal aBMD: an in vivo HR-pQCT study. J Bone Miner Res. 2010; 25:882–890. [PubMed: 19839766]

17. Burghardt AJ, Buie HR, Laib A, Majumdar S, Boyd SK. Reproducibility of direct quantitative measures of cortical bone microarchitecture of the distal radius and tibia by HR-pQCT. Bone. 2010; 47:519–528. [PubMed: 20561906]

18. Macdonald HM, Nishiyama KK, Kang J, Hanley DA, Boyd SK. Age-related patterns of trabecular and cortical bone loss differ between sexes and skeletal sites: a population-based HR-pQCT study. J Bone Miner Res. 2011; 26:50–62. [PubMed: 20593413]

19. Stein EM, Liu XS, Nickolas TL, Cohen A, Thomas V, McMahon DJ, Zhang C, Yin PT, Cosman F, Nieves J, Guo XE, Shane E. Abnormal microarchitecture and reduced stiffness at the radius and tibia in postmenopausal women with fractures. J Bone Miner Res. 2010; 25:2572–2581. [PubMed: 20564238]

20. Mueller TL, Stauber M, Kohler T, Eckstein F, Muller R, van Lenthe GH. Non-invasive bone competence analysis by high-resolution pQCT: an in vitro reproducibility study on structural and mechanical properties at the human radius. Bone. 2009; 44:364–371. [PubMed: 19027092]

21. Boyd SK. Site-specific variation of bone micro-architecture in the distal radius and tibia. J Clin Densitom. 2008; 11:424–430. [PubMed: 18280194]

22. Mueller TL, van Lenthe GH, Stauber M, Gratzke C, Eckstein F, Muller R. Regional, age and gender differences in architectural measures of bone quality and their correlation to bone mechanical competence in the human radius of an elderly population. Bone. 2009; 45:882–891. [PubMed: 19615477]

23. Sode M, Burghardt AJ, Kazakia GJ, Link TM, Majumdar S. Regional variations of gender-specific and age-related differences in trabecular bone structure of the distal radius and tibia. Bone. 2010; 46:1652–1660. [PubMed: 20188877]

24. Burghardt AJ, Kazakia GJ, Sode M, de Papp AE, Link TM, Majumdar S. A longitudinal HR-pQCT study of alendronate treatment in post-menopausal women with low bone density: Relations between density, cortical and trabecular micro-architecture, biomechanics, and bone turnover. J Bone Miner Res. 2010

25. Schnackenburg KE, Macdonald HM, Ferber R, Wiley JP, Boyd SK. Bone Quality and Muscle Strength in Female Athletes with Lower Limb Stress Fractures. Med Sci Sports Exerc. 2011
26. Kazakia GJ, Hyun B, Burghardt AJ, Krug R, Newitt DC, de Papp AE, Link TM, Majumdar S. In vivo determination of bone structure in postmenopausal women: a comparison of HR-pQCT and high-field MR imaging. J Bone Miner Res. 2008; 23:463–474. [PubMed: 18052756]
27. Melton LJ 3rd, Riggs BL, van Lenthe GH, Achenbach SJ, Muller R, Bouxsein ML, Amin S, Atkinson EJ, Khosla S. Contribution of in vivo structural measurements and load/strength ratios to the determination of forearm fracture risk in postmenopausal women. Journal of Bone and Mineral Research. 2007; 22:1442–1448. [PubMed: 17539738]
28. Feldkamp LA, Davis LC, Kress JW. Practical Cone-Beam Algorithm. J Opt Soc Am A. 1984; 1:612–619.
29. Hildebrand T, Rüegsegger P. A new method for the model-independent assessment of thickness in three-dimensional images. Journal of Microscopy. 1997; 185:67–75.
30. Müller R, Ruegsegger P. Three-dimensional finite element modelling of non-invasively assessed trabecular bone structures. Medical Engineering and Physics. 1995; 17:126–133. [PubMed: 7735642]
31. Mueller TL, Christen D, Sandercott S, Boyd SK, van Rietbergen B, Eckstein F, Lochmuller EM, Muller R, van Lenthe GH. Computational finite element bone mechanics accurately predicts mechanical competence in the human radius of an elderly population. Bone. 2011; 48:1232–1238. [PubMed: 21376150]
32. Gross TS, Rubin CT. Uniformity of Resorptive Bone Loss Induced by Disuse. J Orthopaed Res. 1995; 13:708–714.
33. Perrien DS, Akel NS, Dupont-Versteegden EE, Skinner RA, Siegel ER, Suva LJ, Gaddy D. Aging alters the skeletal response to disuse in the rat. Am J Physiol-Reg I. 2007; 292:R988–R996.
34. Belavy DL, Beller G, Ritter Z, Felsenberg D. Bone structure and density via HR-pQCT in 60d bed-rest, 2-years recovery with and without countermeasures. J Musculoskel Neuron. 2011; 11:215–226.
35. Frey-Rindova P, de Bruin ED, Stussi E, Dambacher MA, Dietz V. Bone mineral density in upper and lower extremities during 12 months after spinal cord injury measured by peripheral quantitative computed tomography. Spinal Cord. 2000; 38:26–32. [PubMed: 10762194]
36. Sievanen H. Immobilization and bone structure in humans. Arch Biochem Biophys. 2010; 503:146–152. [PubMed: 20637174]
37. Vico L, Lafage-Proust MH, Alexandre C. Effects of gravitational changes on the bone system in vitro and in vivo. Bone. 1998; 22:95s–100s. [PubMed: 9600761]
38. Rittweger J, Simunic B, Bilancio G, De Santo NG, Cirillo M, Biolo G, Pisot R, Eiken O, Mekjavic IB, Narici M. Bone loss in the lower leg during 35 days of bed rest is predominantly from the cortical compartment. Bone. 2009; 44:612–618. [PubMed: 19168165]
39. Jackson RW, Macnab I. Fractures of the shaft of the tibia; a clinical and experimental study. Am J Surg. 1959; 97:543–557. [PubMed: 13650043]
40. Lamas C, Llusa M, Mendez A, Proubasta I, Carrera A, Forcada P. Intraosseous vascularity of the distal radius: anatomy and clinical implications in distal radius fractures. Hand (N Y). 2009; 4:418–423. [PubMed: 19475457]
41. Nelson GE Jr. Kelly PJ, Peterson LF, Janes JM. Blood supply of the human tibia. J Bone Joint Surg Am. 1960; 42-A:625–636. [PubMed: 13854090]
42. Sheetz KK, Bishop AT, Berger RA. The arterial blood supply of the distal radius and ulna and its potential use in vascularized pedicled bone grafts. J Hand Surg Am. 1995; 20:902–914. [PubMed: 8583061]
43. Kontulainen SA, Macdonald HM, McKay HA. Change in cortical bone density and its distribution differs between boys and girls during puberty. J Clin Endocrinol Metab. 2006; 91:2555–2561. [PubMed: 16636118]
44. Lai YM, Qin L, Hung VW, Chan KM. Regional differences in cortical bone mineral density in the weight-bearing long bone shaft--a pQCT study. Bone. 2005; 36:465–471. [PubMed: 15777653]

45. Rantalainen T, Nikander R, Heinonen A, Daly RM, Sievanen H. An open source approach for regional cortical bone mineral density analysis. J Musculoskelet Neuronal Interact. 2011; 11:243–248. [PubMed: 21885899]

46. Cervinka T, Rittweger J, Hyttinen J, Felsenberg D, Sievanen H. Anatomical sector analysis of load-bearing tibial bone structure during 90-day bed rest and 1-year recovery. Clin Physiol Funct Imaging. 2011; 31:249–257. [PubMed: 21672131]

47. Nagaraja S, Couse TL, Guldberg RE. Trabecular bone microdamage and microstructural stresses under uniaxial compression. J Biomech. 2005; 38:707–716. [PubMed: 15713291]

Highlights

- We characterize spatial variability in cortical structure using HR-pQCT.
- We evaluate 146 male and female volunteers spanning from 20 to78 years of age.
- Significant regional variation exists in all thickness and porosity parameters.
- Regional analysis identifies areas with increased sensitivity to gender and aging.

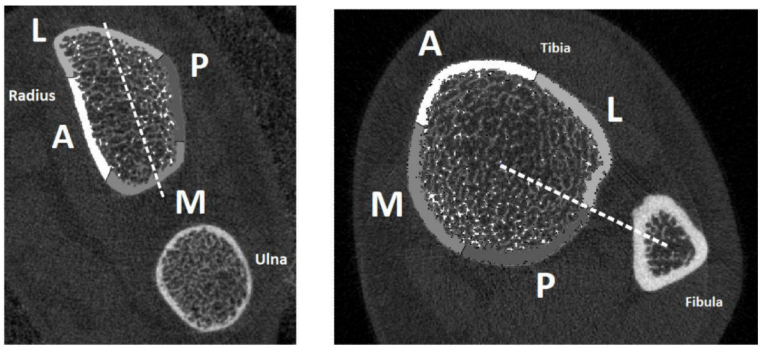

Figure 1.

Definition of regions in the distal radius (left) and tibia (right), with anatomic orientation denoted as A (anterior), P (posterior), M (medial), and L (lateral). Four cortical subregions were defined for each bone based on a reference axis, shown as a dashed line. For the tibia, the line connecting the centroids of the tibia and the fibula cross-sections was used as a reference. For the radius, the major axis of the cross-section was used as the reference, and the quadrants were placed at a 45° offset.

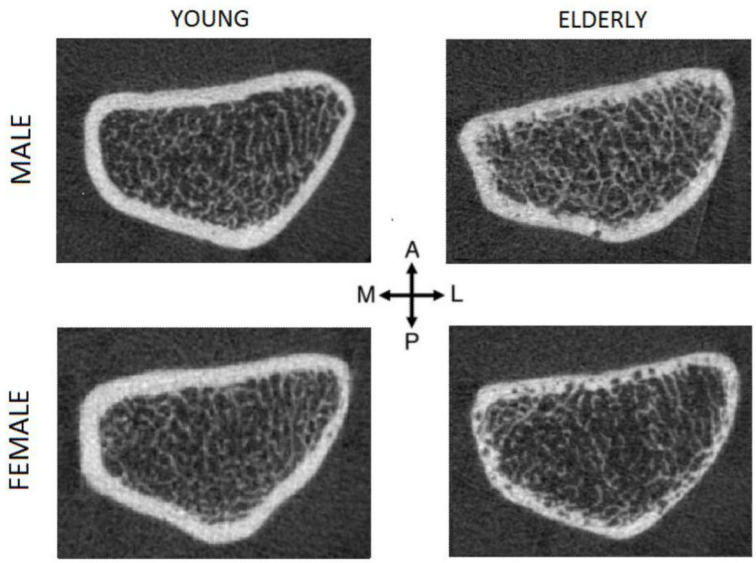

Figure 2.
Representative HR-pQCT images of the radius from young (left) and elderly (right) males (top) and females (bottom).

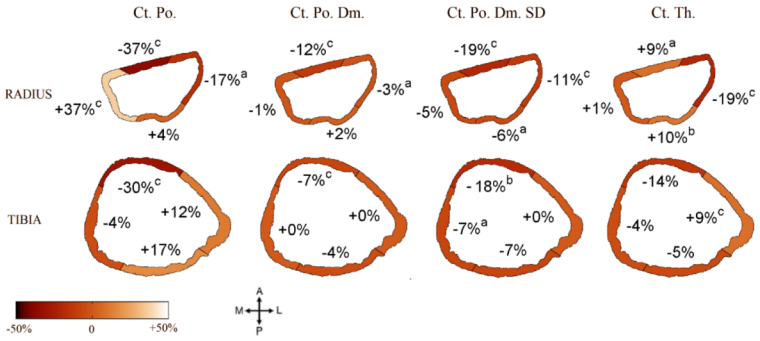

Figure 3.

The mean percent difference from the global mean in cortical indices in each subregion in the distal radius (N=140, top) and tibia (N=145, bottom), inclusive of all subjects. Significant regional variation was detected in cortical porosity (Ct.Po), mean pore diameter (Ct.Po.Dm), heterogeneity of pore diameter (Ct.Po.Dm.SD), and cortical thickness (Ct.Th). Significant differences from the global mean noted as: [a] $p<0.05$, [b] $p<0.01$, [c] $p<0.001$ using Wilcoxon rank-sum tests.

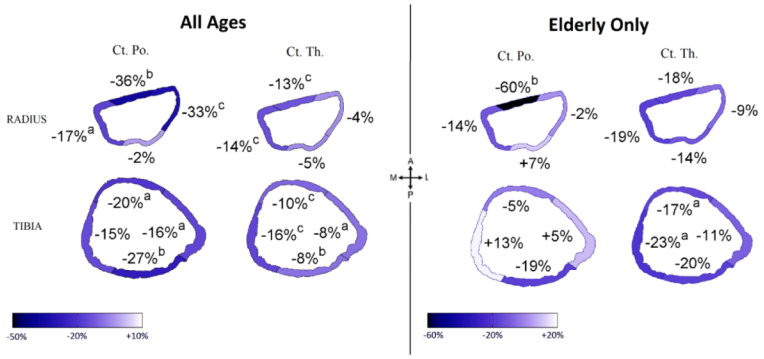

Figure 4.

The mean percent difference in cortical indices for women compared to men of all ages (left, N=86/54 M/F for radius, N=92/53 M/F for tibia) and for the elderly cohort (right, N=9/11 M/F for radius, N=9/13 M/F for tibia) in each subregion of the distal radius (top) and tibia (bottom). Few significant differences in Ct.Po.Dm and Ct.Po.Dm.SD were observed between genders, but patterns in regional variation were generally similar to those of Ct.Po. Significant difference between genders noted as: [a] $p<0.05$, [b] $p<0.01$, [c] $p<0.001$ using Wilcoxon rank-sum tests.

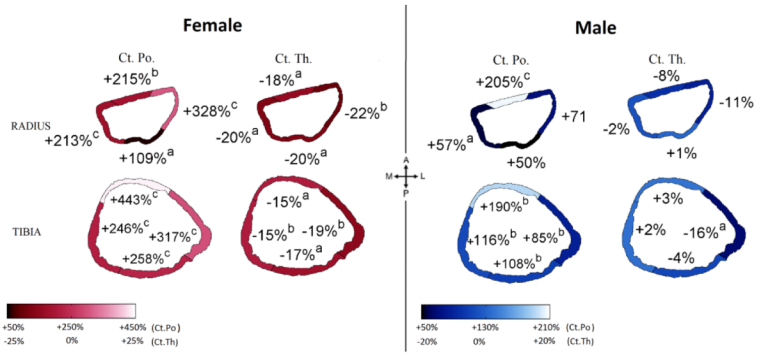

Figure 5.

The mean percent difference in cortical indices for the elderly cohort compared to the young cohort for women (left, N=14/11 Y/E for radius, N=16/13 Y/E for tibia) and men (right, N=11/9 Y/E for radius, N=13/9 Y/E for tibia) in each subregion of the distal radius (top) and tibia (bottom). Variation between age groups in Ct.Po.Dm. and Ct.Po.Dm.SD was rarely significant and with a pattern analogous to that of Ct.Po. Significant difference between cohorts noted as: [a] $p<0.05$, [b] $p<0.01$, [c] $p<0.001$ using Wilcoxon rank-sum tests.

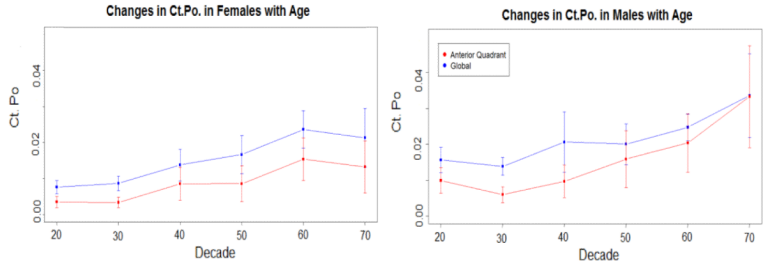

Figure 6.

Changes in Ct.Po with age for males (right) and females (left) globally (blue) and in the anterior quadrant of the radius (red). Women show comparable increases across quadrants in porosity as they age. Men also show comparable change across quadrants, except in the anterior radius, where porosity accelerates with age relative to other quadrants. Error bars denote one standard deviation from the mean.

Table 1

Summary of subject numbers by gender, decade, and anatomic site. The subjects consisted of 146 volunteers (92 females/54 males). Subject ages ranged from 20 to 78 years.

		Decade						
Sex	**Site**	**20**	**30**	**40**	**50**	**60**	**70**	**Total**
Female	Radius	14	14	12	22	17	7	86
	Tibia	16	16	14	21	18	7	92
Male	Radius	11	13	6	13	8	3	54
	Tibia	13	13	5	11	8	3	53

Table 2

Summary of Ct.Po and Ct.Th in young and elderly women and men at the distal radius and tibia.

Ct.Po (%)	**Women**				**Men**			
	Mean ± SD		**Y vs. E diffs**		**Mean ± SD**		**Y vs. E diffs**	
	Young	**Elderly**	**Abs**	**%**	**Young**	**Elderly**	**Abs**	**%**
Radius								
N	14	11			11	9		
Global	0.76 ± 0.34	2.34 ± 1.03	+1.68	+206c	1.55 ± 0.62	2.76 ± 0.70	+1.21	+78[c]
Anterior	0.35 ± 0.28	1.11 ± 0.72	+0.76	+215[b]	0.91 ± 0.59	2.76 ± 1.18	+1.86	+205[c]
Posterior	1.21 ± 0.61	2.52 ± 2.02	+1.32	+109[a]	1.57 ± 0.82	2.36 ± 1.10	+0.82	+50
Medial	0.96 ± 0.50	3.00 ± 1.52	+2.04	+213c	2.21 ± 1.05	3.48 ± 1.22	+1.27	+57[a]
Lateral	0.52 ± 0.29	2.23 ± 1.16	+1.71	+328c	1.30 ± 0.55	2.23 ± 0.76	+0.93	+71[b]
Tibia								
N	16	13			13	9		
Global	1.91 ± 1.11	7.59 ± 3.06	+5.68	+297c	3.72 ± 1.58	7.70 ± 3.10	+3.98	+107[c]
Anterior	1.10 ± 0.86	5.97 ± 3.34	+4.87	+443c	2.17 ± 1.55	6.28 ± 3.65	+4.12	+190[b]
Posterior	2.11 ± 1.43	7.56 ± 3.38	+5.45	+258c	4.48 ± 2.76	9.31 ± 4.48	+4.83	+108[b]
Medial	2.25 ± 1.45	7.82 ± 3.69	+5.56	+246c	3.21 ± 1.88	6.94 ± 3.85	+3.72	+116[b]
Lateral	2.08 ± 1.20	8.66 ± 3.54	+6.59	+317c	4.47 ± 2.16	8.27 ± 3.42	+3.80	+85[b]
Ct.Th(mm)	Women				Men			
	Mean ± SD		Y vs. E diffs		Mean ± SD		Y vs. E diffs	
	Young	Elderly	Abs	%	Young	Elderly	Abs	%
Radius								
N	14	11			11	9		
Global	0.997 ± 0.166	0.797 ± 0.155	−0.200	−20[b]	0.987 ± 0.139	0.951 ± 0.198	−0.036	−4
Anterior	1.062 ± 0.181	0.868 ± 0.200	−0.194	−18[a]	1.139 ± 0.189	1.051 ± 0.245	−0.087	−8

Ct.Po (%)	Women				Men			
	Mean ± SD		Y vs. E diffs		Mean ± SD		Y vs. E diffs	
	Young	Elderly	Abs	%	Young	Elderly	Abs	%
Posterior	1.115 ± 0.219	0.889 ± 0.195	−0.226	−20[a]	1.027 ± 0.128	1.040 ± 0.265	+0.008	+1
Medial	0.988 ± 0.189	0.791 ± 0.157	−0.197	−20[a]	0.987 ± 0.192	0.972 ± 0.228	−0.015	−2
Lateral	0.845 ± 0.150	0.660 ± 0.154	−0.185	−22[b]	0.814 ± 0.100	0.722 ± 0.140	−0.092	−11
Tibia								
N	16	13			13	9		
Global	1.341 ± 0.169	1.112 ± 0.246	−0.222	−17[b]	1.442 ± 0.241	1.349 ± 0.227	−0.093	−6
Anterior	1.280 ± 0.161	1.087 ± 0.233	−0.193	−15[a]	1.339 ± 0.256	1.304 ± 0.151	−0.035	+3
Posterior	1.276 ± 0.173	1.053 ± 0.282	−0.223	−17[a]	1.347 ± 0.201	1.301 ± 0.229	−0.046	−4
Medial	1.284 ± 0.190	1.093 ± 0.307	−0.191	−15[b]	1.395 ± 0.361	1.422 ± 0.338	+0.037	+2
Lateral	1.477 ± 0.021	1.191 ± 0.241	−0.285	−19[b]	1.591 ± 0.282	1.331 ± 0.235	−0.260	−16[a]

Significant differences noted as:

using Wilcoxon rank-sum tests.

[a] $p<0.05$

[b] $p<0.01$

[c] $p<0.001$

Table 3

Spearman correlations between regional cortical structure and biomechanical parameters at the tibia.

	Load distribution	Stress distribution
Ct.Th	0.45	−0.31
Ct.Po	−0.10[p<0.01]	0.56
Tb.BMD	−0.19	0.03[NS]
Tb.N	−0.28	0.22
Tb.Sp.SD	0.23	−0.21

Spearman correlations p<0.001 except as noted

Table 4

Spearman's correlation coefficients for cortical structure indices and age in each region for women and men.

Spearman's	Ct.Po		Ct.Th	
ρ	Women	Men	Women	Men
Radius				
N	86	54	86	54
Global	0.67[c]	0.50[c]	−0.49[c]	0.09
Anterior	0.52[c]	0.49[c]	−0.43[c]	0.03
Posterior	0.36[c]	0.20	−0.45[c]	0.12
Medial	0.62[c]	0.33[a]	−0.43[c]	0.13
Lateral	0.59[c]	0.44[b]	−0.46[c]	−0.7
Tibia				
N	93	53	93	53
Global	0.69[c]	0.57[b]	−0.56[b]	0.05
Anterior	0.73[c]	0.49[c]	−0.38[c]	0.10
Posterior	0.64[c]	0.50[c]	−0.37[c]	0.06
Medial	0.64[c]	0.35[a]	−0.37[c]	0.20
Lateral	0.73[c]	0.45[c]	−0.45[c]	−0.17

Significant correlations noted as:

[a] $p<0.05$

[b] $p<0.01$

[c] $p<0.001$.